







Holocene Palaeoenvironmental and Palaeoproductivity Changes in the Western Amundsen Sea Embayment of Antarctica

Minkyong Kim^{1,2,3} , Jae Il Lee⁴ , Young-Suk Bak⁵, Claus-Dieter Hillenbrand⁶ , Eun Jin Yang⁴ , Daniel B. Montluçon², Negar Haghpor^{2,7}, Timothy I. Eglinton² , and Jeomshik Hwang³ 

¹School of Earth System Sciences, College of Natural Sciences, Kyungpook National University, Daegu, South Korea,

²Geological Institute, Swiss Federal Institute of Technology Zürich (ETHZ), Zürich, Switzerland, ³School of Earth and Environmental Sciences/Research Institute of Oceanography, Seoul National University, Seoul, South Korea, ⁴Korea Polar Research Institute, Incheon, South Korea, ⁵Jeonbuk National University, Jeonju, South Korea, ⁶British Antarctic Survey, Cambridge, UK, ⁷Laboratory for Ion Beam Physics, ETHZ, Zürich, Switzerland

Key Points:

- Polynya-like conditions similar to current conditions were established ~9.2 cal. ka BP in the inner shelf
- Higher rates of deposition of organic carbon on the inner than outer shelf has persisted throughout the Holocene
- Biogeochemical proxies in sediment cores reflect climate oscillations during the early, middle, and late Holocene

Supporting Information:

Supporting Information may be found in the online version of this article.

Correspondence to:

J. Hwang,
jeomshik@snu.ac.kr

Citation:

Kim, M., Lee, J. I., Bak, Y.-S., Hillenbrand, C.-D., Yang, E. J., Montluçon, D. B., et al. (2023). Holocene palaeoenvironmental and palaeoproductivity changes in the western Amundsen Sea Embayment of Antarctica. *Journal of Geophysical Research: Oceans*, 128, e2023JC019797. <https://doi.org/10.1029/2023JC019797>

Received 2 MAR 2023
Accepted 1 MAY 2023

Author Contributions:

Conceptualization: Minkyong Kim, Jeomshik Hwang
Formal analysis: Jae Il Lee, Young-Suk Bak, Daniel B. Montluçon, Negar Haghpor
Funding acquisition: Jeomshik Hwang
Investigation: Minkyong Kim, Eun Jin Yang
Methodology: Minkyong Kim, Jae Il Lee, Young-Suk Bak, Daniel B. Montluçon, Negar Haghpor
Supervision: Jae Il Lee, Claus-Dieter Hillenbrand, Eun Jin Yang, Timothy I. Eglinton, Jeomshik Hwang
Visualization: Minkyong Kim, Young-Suk Bak
Writing – original draft: Minkyong Kim

Abstract The Amundsen Polynya (AP) on the inner and middle continental shelf of the western Amundsen Sea Embayment is the fourth largest coastal polynya around Antarctica. The AP is highly productive when it opens in austral summer, with ~20 times greater organic carbon accumulation rates over the last few thousand years compared to those at nearby shelf sites with more persistent seasonal sea-ice cover. We examined sedimentary records at a site from the AP and another site from the outer shelf to investigate temporal variations in the depositional environment with a special focus on the timing of the AP opening since the deglaciation following the Last Glacial Maximum (LGM; ca. 23–19 cal. ka BP). In the AP region, sedimentological and biogeochemical proxy data reveal a transition from a sub-glacial to a sub-ice shelf and then seasonally open marine conditions comparable to those at present. Total organic carbon contents and diatom valve abundances during the seasonally open marine period imply that the polynya environments was reached at ca. 9.2 cal. ka BP. Since the post-LGM deglaciation, diatom productivity and assemblages in the AP region appear to have varied in association with the variation in the physical environment. Compared to the AP site, only small amounts of organic carbon accumulated on the outer shelf. Differences in the depositional environments and productivity modes between the inner and outer shelf sites have persisted since ca. 10.5 cal. ka BP.

Plain Language Summary The Amundsen Polynya (AP) on the Amundsen Sea shelf is the fourth largest and the most productive coastal polynya around Antarctica. For the last few thousand years, the AP has maintained higher organic carbon accumulation rates compared to nearby sites outside of the polynya. We examined two sediment core records (one from the AP and one from a region with more persistent seasonal sea-ice cover) to track temporal variations in biological production and organic carbon accumulation. A comparison of the sediment records reveals that the differences in the depositional environments and productivity modes between the inner and outer shelf sites have persisted since the grounded ice retreat from the shelf following the Last Glacial Maximum. This finding stresses the importance of polynyas with regard to organic carbon production and the accumulation of seabed sediments around Antarctica. Understanding variability in the past will provide useful information for predicting future environmental and ecological changes in Antarctic polynyas in response to global warming and the resulting sea-ice and glacial ice melting.

1. Introduction

1.1. Physical Environment in the Western ASE

Antarctic coastal polynyas are near-shore shelf areas where the duration of sea-ice-cover is drastically reduced when compared to surrounding shelf regions that experience open-water conditions of only up to a few weeks or months during austral spring and summer (e.g., Martin, 2001). They are characterized by high primary production (PP), especially in summer (Arrigo and Van Dijken, 2003; Smith & Barber, 2007) and are potentially important sites for atmospheric CO₂ absorption (Arrigo et al., 2008).

The Amundsen Sea Embayment (ASE) is located on the West Antarctic continental shelf between the Ross Sea and the Bellingshausen Sea (Figure 1). This region hosts two polynyas, the Pine Island Polynya (PIP) in the east and the Amundsen Polynya (AP) in the west. The AP begins to expand in early November, when the sea-ice

Writing – review & editing: Minkyoung Kim, Jae Il Lee, Young-Suk Bak, Claus-Dieter Hillenbrand, Eun Jin Yang, Timothy I. Eglinton, Jeomshik Hwang

concentration starts to decrease, and can reach a size of $\sim 27,000 \text{ km}^2$ for 132–182 days, whereas the surrounding shelf regions are covered with sea-ice most of the year (Arrigo et al., 2012; Mu et al., 2014). The sea-ice concentration in the Amundsen Sea has decreased over recent decades, a trend that may continue into the future (Parkinson, 2019; Stammerjohn et al., 2012). Ice-shelf melting may result in a loss of grounded ice further upstream (Paolo et al., 2015; Rignot et al., 2013, 2019). This ice-shelf melting is mainly driven by warm, saline Circumpolar Deep Water (CDW) that undergoes upwelling at the continental slope and intrudes far onto the ASE shelf (e.g., Dutrieux et al., 2014; Jacobs et al., 2011; Yang et al., 2022). There are three main water masses characterized on the ASE: modified Circumpolar Deep Water (mCDW) lies below a water depth of ca. 300–600 m, Antarctic Surface Water (AASW) exists at the surface (upper ca. 50–100 m), and Winter Water (WW) is between these two (Dutrieux et al., 2014; Jacobs et al., 2011, 2013; Yager et al., 2012). CDW flows across the western ASE shelf through the Dotson-Getz Trough and forms mCDW by mixing with the overlying shelf waters and glacial meltwaters (Ha et al., 2014; Jenkins et al., 2010; Miles et al., 2016). Recently, studies based on in situ observations and/or models connected the intrusion of CDW with large-scale climate variabilities such as Southern Annular Mode (SAM) and El Niño–Southern Oscillation, (ENSO), which affect wind patterns, surface air temperatures, and sea-ice conditions (Kim, Yang, et al., 2021; Liu et al., 2004; Nakayama et al., 2018; Turner et al., 2017).

1.2. Biogeochemical Characteristics of the Western ASE

The AP is the most productive polynya around Antarctica (Arrigo et al., 2012; Arrigo and Van Dijken, 2003; Mu et al., 2014). Previous in situ measurements showed that the primary production (PP) in the AP ($\sim 2200 \pm 1400 \text{ mgC m}^{-2} \text{ d}^{-1}$ in summer bloom) was much higher than those at nearby shelf sites outside the polynya (Lee et al., 2012). The observations of high PP in the AP are consistent with the total organic carbon (TOC) accumulation rate calculated for late Holocene sediments underlying the AP, which is $\sim 1.2 \text{ gC m}^{-2} \text{ yr}^{-1}$ since 3.4 cal. ka BP and about 20 times higher than that at a site on the outer shelf (Kim et al., 2016). The accumulation of TOC in sediments underlying the AP was estimated to account for $\sim 90\%$ of the organic carbon burial on the entire western ASE shelf, despite the fact that the AP covers only $\sim 30\%$ of this area (Kim et al., 2016).

In order to make better predictions of potential future changes in PP and carbon cycling in the AP, it is important to study earlier variability in the processes, such as that related to biological productivity and organic carbon burial in the sediments, especially focusing on the temporal development of the AP following the retreat of grounded and floating glacial ice since the Last Glacial Maximum (LGM; ca 19–23 ka BP). Several studies have investigated ice sheet/shelf changes in the ASE during the post-LGM deglaciation (e.g., Hillenbrand et al., 2013; Kirshner et al., 2012; Larter et al., 2014; Smith et al., 2011, 2014). According to chronologies based on the ^{14}C dating of foraminifera, the outermost shelf in the western ASE has been free of grounded ice since at least ~ 22.4 cal. ka BP (calibrated ka before present), and the grounding line had retreated to within ~ 12 km of the present Dotson Ice Shelf front by ~ 11.4 cal. ka BP (Smith et al., 2011). This ^{14}C -based chronology matches the ^{14}C dating of the acid-insoluble fraction of organic matter (AIO) at a nearby core site (Smith et al., 2011). Relative paleomagnetic intensity (RPI) records of sediment cores recovered offshore from the Getz Ice Shelf, within 50 km of the modern calving line, suggest that grounded ice had retreated landward from these sites by ca. 13.0 ka, which is supported by AIO ^{14}C dates from these cores (Hillenbrand et al., 2010).

A few studies have focused on the reconstruction of palaeoenvironmental changes of the ASE shelf in the Holocene (e.g., Kim et al., 2016; Kim, Lim, et al., 2021; Lamping et al., 2020). Hillenbrand et al. (2017) found that the SHWW (Southern Hemisphere Westerly Winds), possibly linked to the SAM, was the major controlling factor of CDW advection onto the ASE shelf in the early Holocene. Lamping et al. (2020) reconstructed the dynamics of the ice shelf and sea-ice-cover in the AP during the last deglaciation on the basis of a multiproxy data set, especially evaluating the use of IPSO₂₅, a biomarker for reconstructing the floating ice cover, and a biomarker for phytoplankton production. While this early Holocene environmental change has been relatively well studied (e.g., Hillenbrand et al., 2017; Larter et al., 2014), the marine records pertaining to the subsequent middle/late Holocene on the ASE are still not well understood (Johnson et al., 2014, 2021; Sproson et al., 2022). Recently, Kim, Lim, et al. (2021) presented a stepwise environmental shift related to large-scale climate variation, SAM and ENSO, both known to control the ocean heat content over the ASE by affecting the position of the Amundsen Sea Low (ASL) (Clem et al., 2017). These authors mainly focused on the Little Ice Age (LIA; Grove, 2004) and the modern warm period.

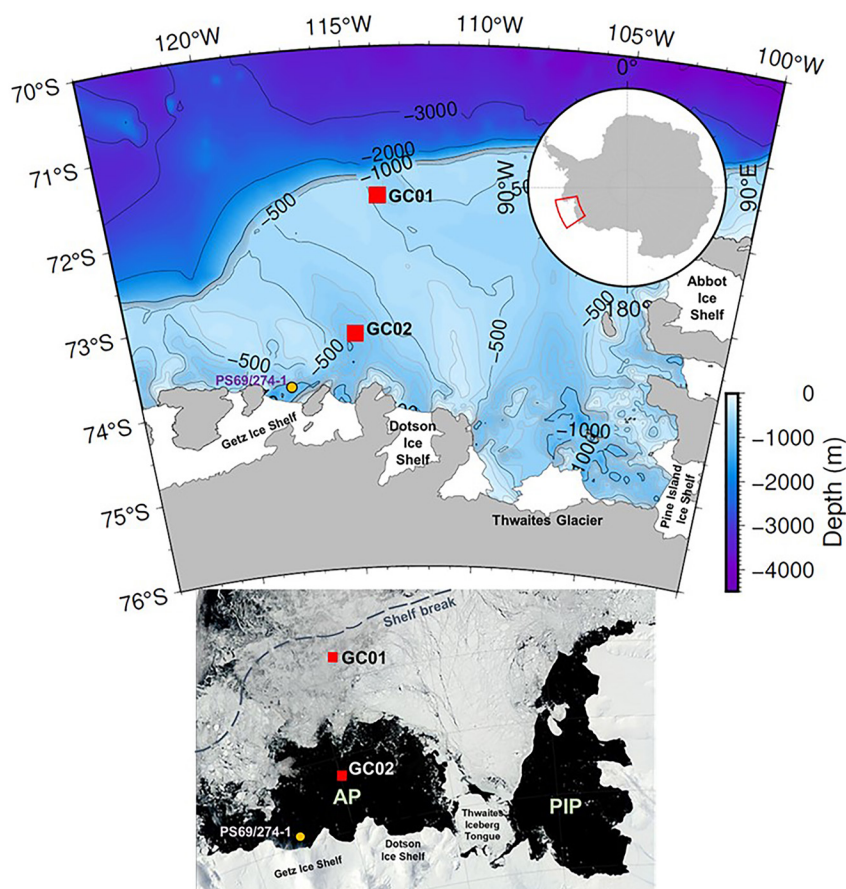


Figure 1. Upper panel: Bathymetric map of the ASE with the locations of the gravity cores analyzed for this study (red squares) and a nearby core previously studied by Lamping et al. (2020) (yellow circle). Lower panel: Satellite image with the sea-ice distribution on 15 February 2022, approximately at the time of core collection for this study. The satellite image was obtained from rapid response imagery from the Land, Atmosphere Near real-time Capability for EOS (LANCE) system, operated by the NASA's GSFC Earth Science Data and Information System (ESDIS). AP and PIP are abbreviations of the Amundsen Polynya and the Pine Island Polynya, respectively. The shelf break is indicated by the dashed line in the image.

In this paper, we reconstruct depositional and related environmental changes in the AP since post-LGM deglaciation using a sedimentary record dated with ^{14}C at a high resolution, thereby focusing on the following questions: (a) When did the AP open for the first time and how did AP development and related sedimentation change over time? (b) How did depositional changes and environmental conditions in the AP area differ from those at a nearby, heavily sea-ice-covered location on the outer shelf?

2. Materials and Methods

Gravity cores with diameters of 12 cm were collected at two locations during a cruise aboard the IBRV *Araon* from January to March of 2012. Site GC01 is located on the outer shelf (71.70°S, 114.04°W; water depth 543 m; recovery 141 cm; original core name AM12-GC01; Figure 1). Site GC02 is located near the center of the AP (73.23°S, 114.91°W; water depth 802 m; recovery 214 cm; AM12-GC02). From each gravity core site, box cores were also collected, for which linear sedimentation rates and other biogeochemical properties were reported previously (Kim et al., 2016).

Gravity core sediments were split into two halves. One half was immediately stored after splitting, and the other half was examined by X-radiography to investigate sedimentary structures (photographic and X-ray images of the cores are presented in Figure S1 in Supporting Information S1). After temperature equilibration overnight, magnetic susceptibility (MS) was measured on the split halves at 1-cm depth intervals using a Bartington MS-2B susceptibility meter mounted on a multisensor core logger (Geotek Ltd., UK). Contents of the elements bromine

(Br) and titanium (Ti) in the sediments were determined with an ITRAX XRF-core scanner, in order to use the Br/Ti ratio as a proxy for marine organic carbon productivity because terrestrial organic matter is relatively poor in Br (e.g., Wu et al., 2019; Ziegler et al., 2008). The samples were scanned from 3 to 50° 2 θ with a scan speed of 5° 2 θ per minute under Ni-filtered CuK α radiation. Sample slices with thicknesses of 1-cm taken at 4-cm depth intervals were analyzed to determine the grain size distribution. Organic matter and carbonate were removed from the samples by treatment with a 5% hydrogen peroxide and 35% HCl solution prior to the grain size measurement. Contents of gravel (>2 mm) and sand (63 μ m–2 mm) were determined by sieving, and the fine fraction (<63 μ m) was analyzed with a SediGraph (Micrometrics SediGraph 5000) to determine contents of silt (2–63 μ m) and clay (<2 μ m). The water content was determined by the difference between the wet and dry weights. The water content of sediment may provide information on the pressure exerted by the mass over the sediment, such as the ice sheet. Another set of 1-cm thick sample slices taken at 2-cm depth intervals was analyzed for total carbon and nitrogen contents using a Flash EA 1112 element analyzer. The CaCO₃ content was calculated from the content of total inorganic carbon measured with a UIC 5030 coulometer. The TOC content was calculated as the difference between the total and inorganic carbon contents. All of these analyses were performed on both cores at the Korea Polar Research Institute (KOPRI).

The radiocarbon (¹⁴C, hereafter) contents of bulk organic carbon in the sediment samples were measured using a gas-ion source Mini Carbon Dating System (MICADAS) accelerator mass spectrometer (AMS) in the Laboratory for Ion Beam Physics at ETH Zürich (Table S1 in Supporting Information S1, Christl et al., 2013; McIntyre et al., 2017). Due to the lack or insufficient amount of calcareous foraminiferas, bulk organic carbon were used for ¹⁴C dating (Figure 2). For this analysis, each finely ground sediment sample was weighed in a silver cup and fumigated with HCl vapor in a desiccator for at least three days at 70°C to remove inorganic carbon. The samples were then stored in a desiccator with NaOH pellets (Fisher Scientific; analytical reagent grade) at 70°C over three days to remove any residual HCl. These samples were converted to CO₂ using an elemental analyzer aligned with the MICADAS. Radiocarbon measurements were normalized using an oxalic acid II standard (NIST SRM 4990C) and corrected for constant contamination introduced during fumigation using in-house shale and soil reference materials according to Haghipour et al. (2019). At each site, we corrected the down-core ¹⁴C dates (in years BP) measured on the gravity core samples by subtracting previously published, uncorrected ¹⁴C dates of bulk organic matter in seafloor surface sediments (0–1 cm) from the box cores collected at the same sites. The corresponding ages were 3860 years (GC01) and 2930 years (GC02) (Kim et al., 2016). The corrected ¹⁴C ages were then converted to calibrated years BP (cal. BP) using the CALIB 8.2 calibration program with the Marine20 data set (<http://calib.org>; Heaton et al., 2020; Reimer et al., 2013; Stuiver & Reimer, 1993).

A set of 1-cm-thick sediment slices (from the core surface to 16 cm depth) and another set of 2-cm-thick slices (from 16 cm depth to the core base) were taken for AMS ¹⁴C dating and for an ICP-AES analysis of aluminum (Al), barium (Ba) and zirconium (Zr). We used the Ba/Al ratios as a proxy for biological productivity and the Zr/Al ratios both as a grain-size proxy because fast bottom current causes relative enrichment of heavy minerals over less dense aluminosilicates (e.g., Bahr et al., 2014) and for evaluating the contribution from terrigenous heavy minerals to the observed down-core Ba/Al changes (e.g., Hillenbrand et al., 2017) (note: some Al quantifications by XRF-scanning were unrealistically low). These subsamples were freeze-dried, and then sieved to remove ice rafted debris (>2 mm, Grobe, 1987) and stored frozen in pre-baked (450°C for 4 hr) glass jars. The element analysis was carried out using an ICP-AES (Optima 8300, PerkinElmer) at the Korea Basic Science Institute, with a relative standard deviation (RSD) of 2.8%, 4.4%, and 7.6% for Al, Ba, and Zr, respectively.

For a sterol analysis, a set of 1-cm-thick sediment slices at depths of every 4-cm was used. Approximately 2–30 g of each freeze-dried and homogenized sample was extracted into a dichloromethane:methanol (90:10 v:v) mixture using a microwave extraction system (MARS6 CEM Corporation; 100°C, 20 min). An internal standard (1-nonadecanol, Sigma-Aldrich, 99%) was added prior to the analytical treatment for a reproducibility check. Sterols were quantified by comparison to an external cholesterol standard (Sigma-Aldrich, \geq 99%). The total lipid fraction was separated into three fractions by silica gel column chromatography using hexane, hexane:ethyl acetate (75:25 v:v), and methanol. The second fraction was silylated with bistrimethylsilyl-trifluoroacetamide (BSTFA) and pyridine at 70°C for 30 min. Derivatized fractions were injected into an Agilent 7890A gas chromatograph equipped with a capillary column (DB-1MS, 0.32 ID, 30 m length). Peaks were detected and quantified with a time-of-flight mass spectrometer (TOF-MS; ALMSCO-BenchTOF-dx; 70 eV constant ionization potential). The gas chromatograph analysis was performed with the following temperature program: 40°C (1 min),

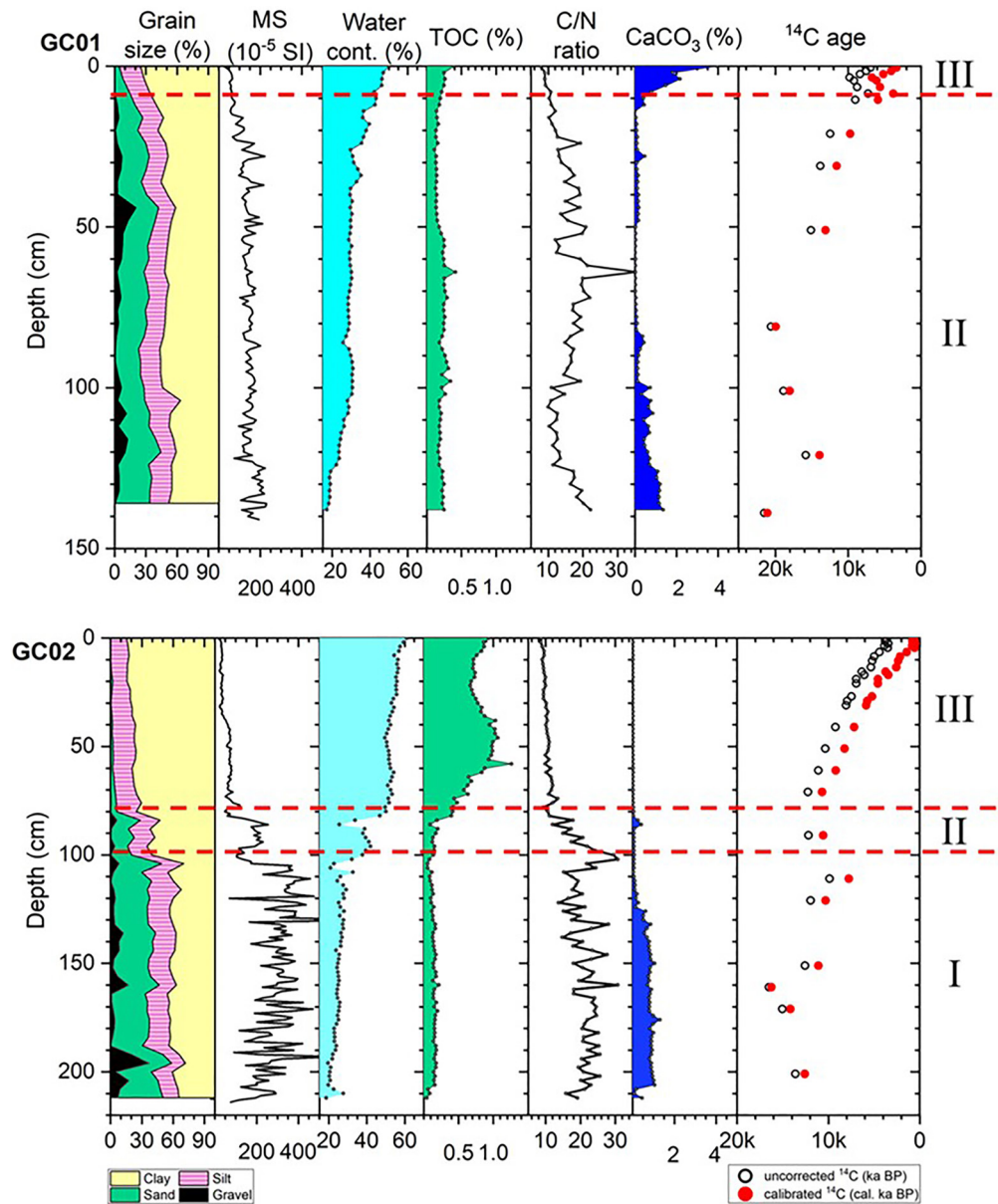


Figure 2. Vertical distribution of sedimentological and geochemical proxies, ^{14}C ages of organic matter of cores GC01 (top) and GC02 (bottom). MS stands for magnetic susceptibility. Uncorrected ^{14}C ages indicate the apparent ^{14}C ages of bulk organic matter (ka BP; open circles) and calibrated ^{14}C ages indicate the reservoir effect-corrected and calibrated kilo-years BP (cal. ka BP; closed circles).

130°C (rate: 40°C/min.), 320°C (rate: 10°C/min.), 320°C (10 min). The injection volume was 1 μl in the splitless mode. Individual sterols were identified based on their mass spectra and retention times.

In this paper, GC02 collected from the central AP as the prime core covers temporal variations from sub-glacial to seasonal open marine environment and diatom assemblages were investigated only on this core (Figure 2, Table S2 in Supporting Information S1). For the quantification of diatom abundances and diatom taxon identification, an amount of ~ 2 g of dry sediment from a set of 1-cm thick sediment slices taken at 4-cm depth intervals was used. The samples were heated to 100°C with 25 ml of hydrogen peroxide (H_2O_2 , 30%) and 25 ml of 10% hydrochloric acid for 1 day to oxidize the organic matter and dissolve the carbonates (Bak et al., 2018). Samples were then washed three times with distilled water. Slides for diatom counting were prepared using the random settling method of Scherer (1994), and the Norland optical adhesive (No. 61, refractive index: 1.56) was used as a

mounting medium. Diatom counting and identification were conducted using a Nikon E400 microscope at 1000X magnification (Esper et al., 2010; Gersonde & Zielinski, 2000; Heiden & Kolbe, 1928; Hustedt, 1930-1966, 1958; Johansen & Fryxell, 1985; Manguin, 1957, 1960; Medlin & Priddle, 1990; Peragallo, 1921; Simonsen, 1992).

3. Results and Discussion

3.1. Radiocarbon Chronology

We examined the possibility of the loss of seafloor surface sediments during gravity coring by comparing the core top ^{14}C ages and down-core variations of the ^{14}C ages, C/N ratios and contents of TOC and CaCO_3 of the gravity cores to those of the box cores recovered from the same sites, for which preservation of seafloor surface sediments had been confirmed visually (Figure S2 in Supporting Information S1; Table S3; Kim et al., 2016). At site GC01, the CaCO_3 content and its down-core variations were the most useful parameter for comparison. Approximately the top 7 cm of the gravity core appeared to have been lost during the coring process (Figure S2 in Supporting Information S1). At site GC02, the TOC content and its down-core variations were the most useful parameter for comparison. Approximately the top 12 cm of the gravity core appeared to have been lost in this case (Figure S2 in Supporting Information S1).

At site GC02, there are down-core age reversals at depths of 17 cm, 91 cm, 111–121 cm, and 171–201 cm (Figure 2, Table S1 in Supporting Information S1). Together with the relatively old ^{14}C ages, these reversals indicate variable and relatively large contributions from reworked fossil organic carbon in the core layer deeper than 100 cm (cf. Hillenbrand et al., 2010; Smith et al., 2011); therefore, we consider the ^{14}C ages of this deeper layer as unreliable. In comparison, the ^{14}C ages in the top layer down to 82 cm increase nearly continuously with an increase in the core depth and lack major age reversals (only one reversal is observed). Thus, we believe that the ^{14}C ages in the top 82 cm layer are reliable. Age reversals were also observed at 6.5–10.5 and 121 cm of core GC01.

3.2. Reconstruction of Depositional Environment

We focus the following discussion of the changes in the sedimentation environments in the AP area inferred from proxies analyzed on core GC02, and then compare them to those at site GC01. We spliced the box core data with the data from the gravity cores but we refer to the gravity core depth scale below only in order to avoid confusion.

3.2.1. Temporal Variation in Sedimentation in the AP Region (GC02)

The most conspicuous changes were the sudden up-core decrease in the content of coarse sediment (grain size), the magnetic susceptibility, and the C/N ratio, and the sudden increase in the water content. Based mainly on the grain size distribution, magnetic susceptibility, and water content, sediment core GC02 is divided into three units (Figures 2, 3 and Figure S1 in Supporting Information S1).

Unit I: Sub-Glacial to Grounding-Line Proximal Sub-Ice Shelf Deposition

Unit I from the core base at a depth of 214–100 cm is sandy, gravelly mud with ~40 wt.% of gravel and sand. Unit I is laminated throughout, but there is one burrow at a depth of ~110 cm (Figure S1 in Supporting Information S1). High and highly variable MS values reflect the coarse sediment grain sizes (e.g., Kim et al., 2022; Leventer et al., 1996). The water content is lowest in Unit I (mean = 25%), indicates that the sediment is under the pressure. High C/N ratios with considerable variation (mean = 21 ± 4) indicate that the organic matter was predominantly terrestrial in origin, while the CaCO_3 contents (~0.66%) reflect the presence of either very fine-grained, reworked, fossil biogenic debris or detrital carbonate (Figure 2). Diatom valves were virtually absent in this unit, indicating insignificant plankton productivity during its deposition (Figure S3 and Table S2 in Supporting Information S1). We propose that Unit I was deposited in a sub-glacial/grounding-line proximal sub-ice shelf condition.

Unit II: Grounding-Line Distal Sub-Ice Shelf or Permanent Sea-Ice Deposition

Overlying Unit II (100–82 cm) is stratified and slightly bioturbated sandy, silty clay with ~18 wt.% sand and little gravel. The TOC content in Unit II increased from 0.1% to 0.4%, and the C/N ratio decreased from ~30 to 11 up-core, suggesting that Unit II is concomitant with the onset of significant marine PP and the deposition of fresh marine organic matter (Figure 2). However, diatom valve abundance as a proxy for in situ PP was very

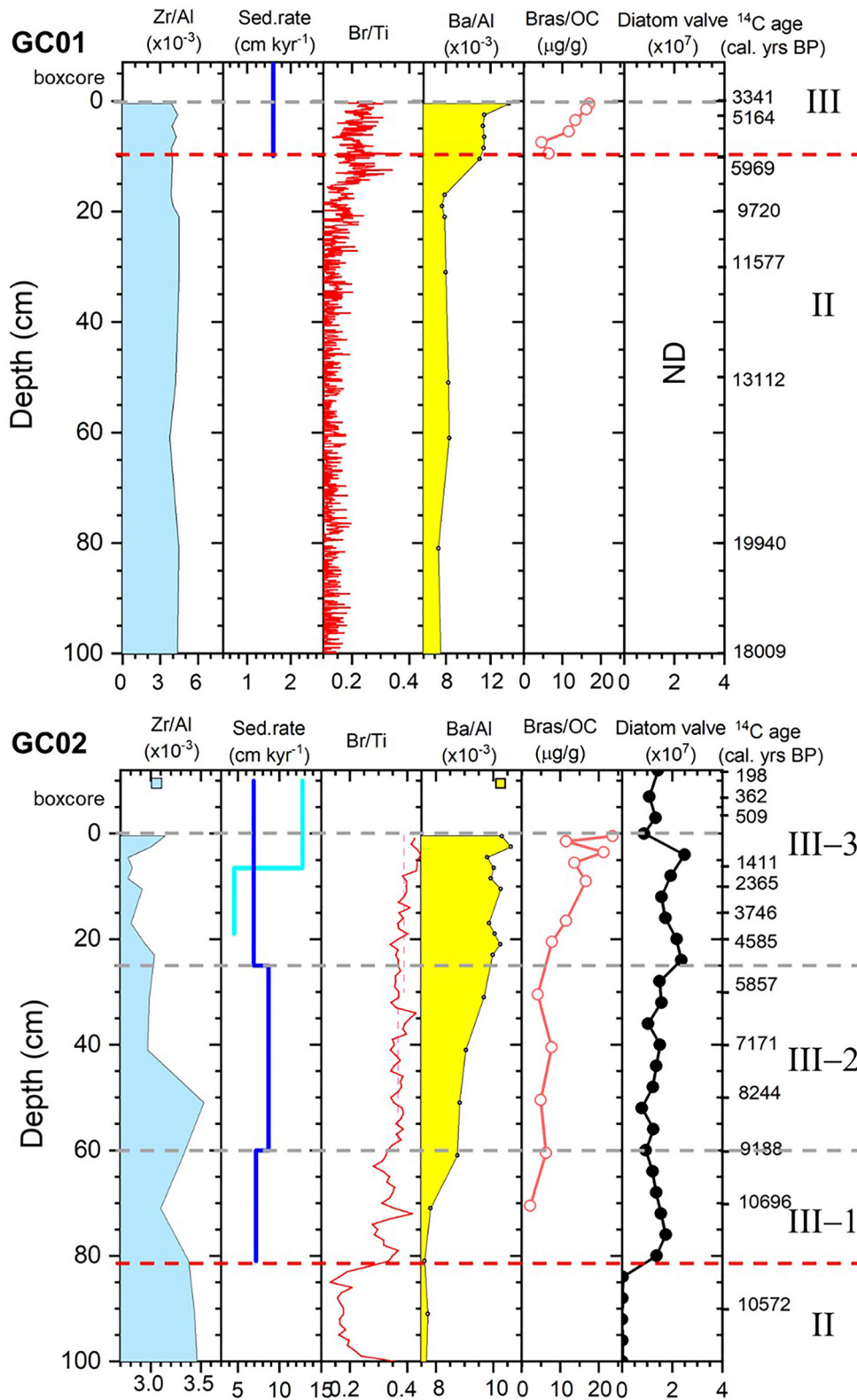


Figure 3.

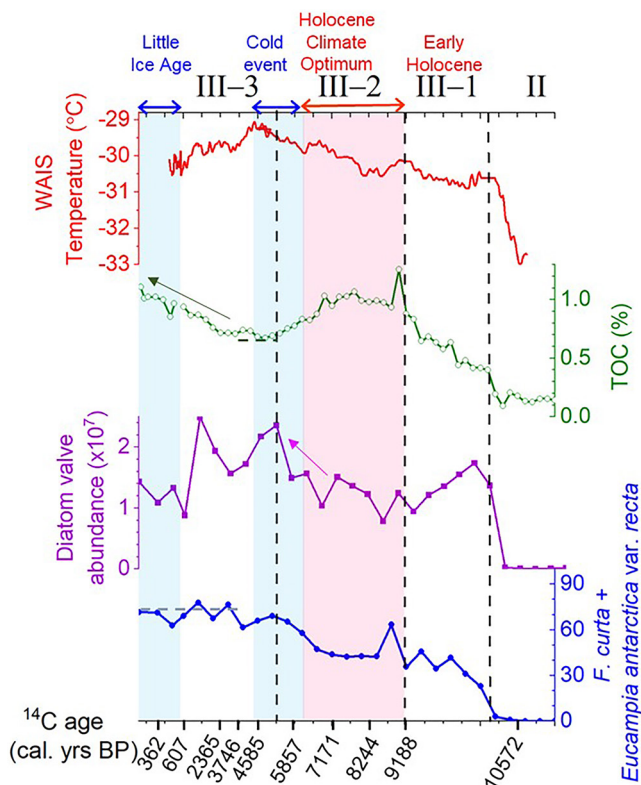


Figure 4. Downcore changes in air temperature ($^{\circ}\text{C}$) recorded in the West Antarctic Ice Sheet Divide ice core (Cuffey et al., 2016), TOC content (%), total diatom valve abundance, and the sum of *F. curta* and *E. antarctica* var. *recta* abundances in core GC02. The shadings denote cold (blue) and warm (red) climatic events in the Antarctic realm; Holocene Climate Optimum (Sproson et al., 2022), cold event (Björck et al., 1996; Yoon et al., 2000), and Little Ice Age (Bertler et al., 2011).

low ($<0.03 \times 10^7$ valve g^{-1} ; Figures 3 and 4). Particulate organic matter produced seaward of an ice shelf front in the seasonally open marine environment may therefore have been advected under an ice shelf before its deposition and thereby sustained a sub-ice shelf benthic community, as has been observed for some modern Antarctic ice shelves (e.g., Riddle et al., 2007; Smith et al., 2019). The Ba/Al ratio, a proxy for palaeoproductivity (e.g., Hillenbrand et al., 2017), is also low (~ 0.008) in Unit II (Figure 3). We propose that Unit II was deposited in a distal sub-ice shelf or permanent sea-ice condition (Figures 2 and 3).

Unit III: Seasonal Open Marine Environment

Unit III (82 cm–core top) is silty clay with little sand (6 wt.%) and devoid of gravel. The silt content is fairly constant ($19 \pm 3\%$) in all three units. The clay content is highest in Unit III. MS values are lowest, reflecting low amounts of terrigenous components (e.g., Kim et al., 2022; Leventer et al., 1996). The water content was highest in Unit III (mean = 54%). The boundary of Units II and III has an age of ~ 10.5 cal. ka BP, which is consistent with Larter et al. (2014), indicating that in the ASE, the grounding line of the West Antarctic Ice Sheet was already at a position to similar to that at the present time at ~ 10 cal. ka BP.

In Unit III, the TOC content gradually increased up-core from 0.4% to 1.0%, a value similar to that in the surface sediments of the box core recovered from the same site (Figures 2 and 4). Diatom valve abundance was increased by more than two orders of magnitude at the boundary between Units II and III (from 0.02×10^7 to 1.37×10^7 v g^{-1} ; Figure 3). Glacial-ice associated *Eucampia antarctica* var. *recta* and sea-ice associated *Fragilariopsis curta* were dominant throughout Unit III (Figure S3 in Supporting Information S1). Also, the sea-ice taxon *F. curta* dominated an open-water taxon, *Fragilariopsis kerguelensis*, throughout Unit III. C/N ratios (mean = 10 ± 1) were characteristic for marine organic matter, indicating that in situ PP was the main source of organic matter (Figure 2). We propose that Unit III was deposited in an open (seasonally) marine environment (Figures 2 and 3).

3.2.2. Temporal Variation in Sedimentation in a Heavily Sea-Ice-Covered Region (GC01)

The 141-cm-long core GC01 from the outer shelf showed lithological units different from those in core GC02 (Figure 2). GC01 includes layers only comparable to Units II and III. Unit I, which is observed in GC02, was not recovered in GC01 based on the grain size distribution and the MS (Figure 2 and Figure S1 in Supporting Information S1).

Unit II: Deposition Under a Thick Sea-Ice Cover

The whole core below 10 cm has characteristics similar to those of Unit II of core GC02. The deposition of Unit II likely started at 20–18 cal. ka BP at site GC01 (Figure 2, Table S1 in Supporting Information S1). The water content increased from 17% to 43%, suggesting that GC02 emerged from under the ice shelf at this time (Figure 3). Overall, the grain size and MS values gradually decreased up-core. The C/N ratio was between 10 and 22, whereas there are some fluctuations within the unit. The ratio of Br/Ti, a proxy for marine organic carbon productivity, jumped at 10–16 cal. ka BP (Figure 2). However, the TOC content is similar ($\sim 0.2\%$) throughout Unit II, suggesting that marine PP started, but its intensity (or at least the, deposition of organic carbon) was weak. Thus, site GC01 was likely covered with thick sea-ice during deposition in Unit II.

Figure 3. Vertical distributions of the Zr/Al ratio as a proxy for the contents of coarse grains and heavy minerals, the linear sedimentation rate (cm kyr^{-1}), Br/Ti, Ba/Al, brassicasterol/OC, and the total diatom valve abundances in cores GC01 and GC02. New and previous results of the box core at site GC02 (Kim et al., 2016) are also presented. The blue and yellow square symbols of the Zr/Al and Ba/Al columns in core GC02 indicate values obtained from the boxcore samples. Calibrated ^{14}C ages of bulk organic matter (in cal. yrs BP) are shown on the right y-axis. The red lines indicate the boundary of Unit II and III while the gray lines indicate each boundary of the subunits of Unit III and the gravity core surface.

Unit III: Seasonal Open Marine Environment Under a Thin Sea-Ice Cover

The sand content was sharply decreased, and water content was increased to ~43 wt.% at the boundary between Unit II and III. Only the top 10 cm layer has characteristics similar to those of Unit III in GC02. The deposition of Unit III started around 6.0 cal. ka BP. The water, TOC and CaCO₃ contents gradually increased up-core to values similar to those in the surface sediments of the box core recovered from the same site (Figure 2). Thus, the sea-ice cover presently observed in this region was likely established as late as 6.0 cal. ka BP.

3.2.3. Comparison of Sedimentation Between the AP and the Outer ASE Shelf

Since the onset of the seasonal open marine conditions, ~10 cm of sediment was deposited at site GC01 and ~94 cm was deposited at site GC02. Despite the uncertainty in the age determination of the onset of the Unit III deposition at site GC01, the difference in the linear sedimentation rate (LSR) is clear between GC01 and GC02. The low LSR at site GC01 on the outer shelf could have been caused by sediment winnowing by the bottom currents and/or iceberg scouring (Hillenbrand et al., 2012; Smith et al., 2011). However, iceberg scours were not observed in multibeam bathymetric data collected at the studied site during the aforementioned cruise (Kim, 2012; cf. Graham et al., 2009). Also, current speeds measured within the water column at depths between 400 and 500 m were higher on the inner shelf than on the middle and outer shelf (Kim et al., 2019).

Sedimentation of biogenic material on the seasonally open marine shelf in the western ASE is likely to reflect biological production in the surface waters. The presence of CaCO₃ in Unit III of GC01 contrasts with the absence of CaCO₃ in Unit III of core GC02 (Figure 2 and Figure S1 in Supporting Information S1). This pattern is consistent with modern observations of sinking particles collected in sediment traps (Kim et al., 2015, 2019) and may be due to the planktic foraminifer *Neogloboquadrina pachyderma* sinistral. This species dominates planktic foraminifera assemblages south of the Antarctic Polar Front (e.g., Donner & Wefer, 1994) and is adapted to the sea-ice habitat (e.g., Dieckmann et al., 1991; Thomas et al., 1998). The TOC accumulation rate was 0.15 gC m⁻² yr⁻¹ at GC01 and 0.97 gC m⁻² yr⁻¹ at GC02. Therefore, different modes in marine biological productivity resulting from differences in the sea-ice cover inside and outside of the AP have apparently persisted since the post-LGM retreat of the Dotson-Getz palaeo-ice stream from the shelf.

The inferred onset of seasonally open-marine conditions near the modern coastline is consistent with that in previous studies (Hillenbrand et al., 2010; Lamping et al., 2020; Smith et al., 2011). However, we observed a time transgressive, northward progression of this onset from the earliest until the middle of the Holocene. This can be explained by an early establishment of the AP that allowed primary productivity to develop on the inner shelf. In contrast, dense sea-ice cover persisted on the middle to outer shelf for several thousand years longer, thus delaying the initiation of significant plankton productivity. Also, the present-day annual sea-ice concentration in the western ASE decreases from the outer to the inner shelf (e.g., Macdonald et al., 2023; Stammerjohn et al., 2015).

3.3. Variation in the Biogeochemical Properties and the Potential Linkage to Climate Variability in the Holocene

Based mainly on the variations of the TOC content and diatom species and abundances, we divide Unit III of GC02 into three subunits: Subunit III-1 from 82 to 60 cm (from ca. 10.5 to ca. 9.2 cal. ka BP; earliest Holocene), Subunit III-2 from 60 to 25 cm (from ca. 9.2 to ca. 5.2 cal. ka BP; early middle Holocene), and Subunit III-3 from 25 cm to the sediment surface (from ca. 5.2 cal. ka BP; middle-late Holocene) (Figures 3 and 4).

The onset of the TOC increase and diatom production marking the base of Subunit III-1 coincided with the end of a phase of rapid increases at ~10.5 cal. ka BP in the Antarctic air temperature recorded in the West Antarctic Ice Sheet (WAIS) Divide ice core (WDC) (Figure 4 and Figure S3 in Supporting Information S1; Cuffey et al., 2016; Jones et al., 2023; Ólafur et al., 2003; data obtained from <http://www.usap-dc.org/view/dataset/600377>). The TOC contents (%) increased gradually from <0.3% to ~1% (Figure 4). Total diatom valve abundance increased sharply at the base of Subunit III-1 (Figures 3 and 4), which typifies the onset of seasonally open-marine conditions after the retreat of the ice shelf front (e.g., Domack et al., 2005; McKay et al., 2008). The diatom assemblage was composed mainly of *F. curta*, *E. antarctica* var. *recta*, and *Fragilariopsis obliquecostata* (Figure S3 in Supporting Information S1) and thus documents a strong sea-ice influence (e.g., Armand et al., 2005; Esper & Gersonde, 2014; Fryxell, 1991). We propose that Subunit III-1 represents a transitional stage toward a condition favorable for phytoplankton production during the earliest Holocene. The concomitant changes in the Ba/Al and Br/Ti ratios, which increased sharply from ~0.1 to ~0.4 at the base of the subunit, are consistent with an increase

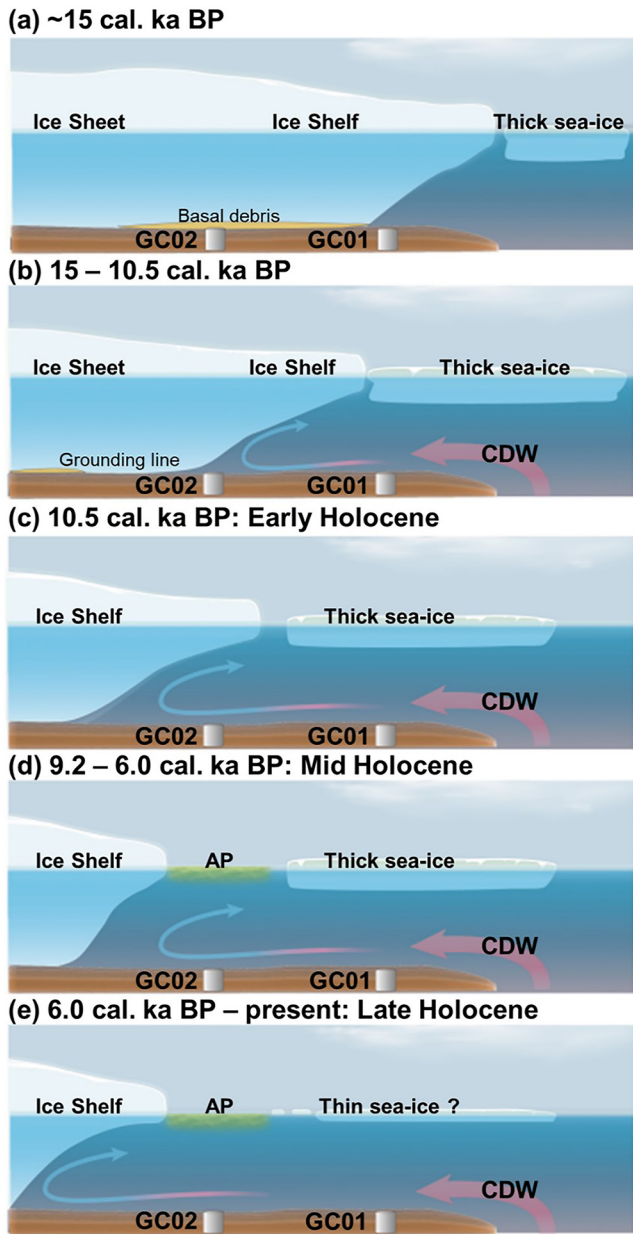


Figure 5. Schematic illustration of the environmental conditions in the western ASE. The phases were divided based on the ice conditions above sites GC01 and GC02 inferred from our multi-proxy analyses.

in phytoplankton production during the earliest Holocene (Figure 3). The ratio of brassicasterol, as an indicator of diatoms and other primary producers (Volkman, 1986), to organic carbon (brassicasterol/OC) started to increase with the deposition of Subunit III-1 (Figure 3). Brassicasterol abundances were very low in both Unit I and Unit II (Figure 4).

Subunits III-2 and III-3 have relatively high and stable TOC contents (0.8% on average) compared to the gradual increase in Subunit III-1, suggesting that high biological productivity at site GC02 has persisted since ca. 9.2 cal. ka BP (Figure 3). This middle/late Holocene period includes climate variations such as the Holocene Climate Optimum and cold periods observed around Antarctica. Based on beryllium isotope, Sproson et al. (2022) reported that the ASE suffered melting and retreat of glaciers between 9 and 6 ka BP forced by atmospheric circulation changes over continental West Antarctica. This period coincides with the climate optimum between 7 and 5 ka BP observed from the eleven ice core records around Antarctica (Masson et al., 2000). The diatom valve abundance increased slightly during this period (Figure 4).

In the middle Holocene, glacial and ice shelf readvances have been reported for several regions in the Antarctic (Ashley et al., 2021; Domack et al., 2001; Yoon et al., 2000). Yoon et al. (2000) reported cold waters and extensive sea-ice cover between 6.2 and 4 ka BP from King George Island. In the Antarctic Peninsula region, Björck et al. (1996) presented a paleoclimatic synthesis of the Holocene and at climate transition from relatively mild and humid condition to cold and arid conditions at ~5 ka BP. This period with cold events corresponds to the early part of subunit III-3, when the TOC content was in a dip. The end of the cold event corresponds to the timing of the increased size (efficiency) of polynyas in the Ross Sea (~3.6 cal. ka BP; Mezgec et al., 2017). After the minimum value in the cold event, the TOC content gradually increased upcore in the AP (Figure 4).

During the LIA, cold sea surface temperatures, increased sea-ice extent, and strong katabatic winds around Antarctica have been suggested (Bertler et al., 2011; Rhodes et al., 2012). The TOC content of GC02 continued to increase during the LIA. The estimated LSR was highest (12.7 cm/kyr; Figure 3), possibly due to the enhanced PP. In the meantime, the diatom valve abundance decreased since ~0.8 ka BP, implying a shift in the phytoplankton species in the AP. At present, *Phaeocystis antarctica* is the dominant primary producer in terms of biomass in the central AP while diatoms are dominant in the shelf regions outside the AP (Yang et al., 2016). Considering the present plankton community, it is suspected that the plankton community in the AP was similar to that at present in this time period.

3.4. Temporal Evolution of the Ice Shelf and Sea-Ice-Cover in the Western ASE

Larter et al. (2014) reconstructed the extent of the grounded WAIS (West Antarctic Ice Sheet) on the ASE and Bellingshausen Sea shelves since 25 cal. ka BP at 5 ka intervals. During the LGM, the grounding line was close to the continental shelf break and the ice sheet retreated landward at 20–15 cal. ka BP. Thus, site GC01 on the outer shelf emerged from a sub-ice shelf position by ~15 cal. ka BP (Fig. 12 in Larter et al., 2014). Gradual ice thinning in the hinterland of the ASE since 14.5 cal. ka BP was also reported by Johnson et al. (2008). From 15 to 10 cal. ka BP, the majority of the ASE shelf was free of grounded ice and the WAIS grounding line had retreated onto the inner shelf (Larter et al., 2014). The grounding line had retreated close to its modern position before 10 cal. ka BP (Fig. 13 in Larter et al., 2014).

Thus, site GC02 was probably located in seasonal open water by this time, corresponding to the start of the deposition of Unit II (10.5 cal. ka BP).

Based on the reconstruction from Larter et al. (2014) and our ^{14}C dates from cores GC01 and GC02, we propose the following environmental changes in the ASE (Figure 5). At ~ 15 cal. ka BP, GC01 became free of grounded ice while GC02 was still located below the ice sheet (Figure 5a). Unfortunately, reliable dating of the older lithological Units I and II in our cores, with Unit II having been deposited in a glacial marine setting, was not possible due to the apparent high and highly variable contributions of reworked fossil organic carbon influencing the bulk organic matter ^{14}C dates. Therefore, we adopt the age for the boundary between Units I–II from Larter et al. (2014) (Figures 5a and 5b). The ice sheet and grounding line continued to retreat from 15 to 10.5 cal. ka BP (Figure 5b), and site GC02 was situated in seasonal open water at ~ 10.5 cal. ka BP (Figure 5c). At this time, GC01 was covered by thick sea-ice. From ~ 9.2 cal. ka BP, seasonal open marine conditions started in the AP (Unit III-2), allowing significant biological production. The outer shelf site GC01 was still covered by thick sea ice (Figure 5d). Environmental conditions similar to those at the present started at ~ 6.0 cal. ka BP: Site GC02 was then located in the highly productive AP (Figure 5e).

4. Conclusion

We have examined sedimentological and palaeoproductivity proxies in two gravity cores obtained from settings with different surface water conditions and sea-ice cover characteristics in the western ASE. The sediment record from the central AP reflects a transition from a sub-glacial/proximal grounding-line sub-ice shelf to a distal sub-ice shelf, and finally to seasonally open marine conditions. We suggest that polynya-like conditions favoring high biological productivity were established subsequent to ice shelf retreat and appear to have persisted since ~ 9.2 cal. ka BP in the central AP based on several productivity proxies. We additionally propose that (a) the biological productivity in the AP was similar to that currently during the time interval from ~ 9.2 cal. ka BP, and (b) the condition of the sea-ice-covered outer shelf similar to the present started at ~ 6.0 cal. ka BP. On the western ASE shelf biological productivity, also expressed by variations in the composition of the plankton community, appears to have changed with the climate variations recorded in the Antarctic. Our results show that the contrasting evolution of environmental conditions and the resulting sediment deposition in the AP and on the outer shelf of the ASE have persisted throughout the late Holocene.

Acknowledgments

We thank Heung Soo Moon for the gravity core sampling and the captain and crew of the IBRV *Araon* for the help at sea. We also thank the staff at the Laboratory for Ion Beam Physics at ETH Zürich for the carbon isotope analysis. This study used rapid response imagery from the Land, Atmosphere Near real-time Capability for EOS (LANCE) system, operated by the NASA's GSFC Earth Science Data and Information System (ESDIS), with funding provided by NASA/HQ. This research was supported by the Korea Polar Research Institute (KOPRI PE23090) grant funded by the Ministry of Oceans and Fisheries. MK was partly supported by Korea Polar Research Institute (KOPRI PE23900) grant funded by the Ministry of Oceans and Fisheries. Basic Science Research Program through the National Research Foundation of Korea (NRF) funded by the Ministry of Science and ICT (2022R1C1C1002824) and the Young Researcher's Exchange Program between Korea and Switzerland (2017K1A3A1A14092122). YSB is funded by the Natural by the National Research Foundation of Korea (NRF) grant funded by the Korea government (MSIT) (No. 2022R1A2C1091796). CDH is funded by the Natural Environment Research Council (NERC), UK.

Data Availability Statement

All data used for this manuscript are available at the National Oceanic and Atmospheric Administration's National Centers for Environmental Information (NCEI) web interface (Kim et al., 2023; <https://doi.org/10.25921/4dss-7784>).

References

- Armand, L. K., Crosta, X., Romero, O., & Pichon, J. J. (2005). The biogeography of major diatom taxa in Southern Ocean sediments. *Palaeogeography, Palaeoclimatology, Palaeoecology*, 223(1–2), 93–126. <https://doi.org/10.1016/j.palaeo.2005.02.015>
- Arrigo, K. R., Lowry, K. E., & van Dijken, G. L. (2012). Annual changes in sea ice and phytoplankton in polynyas of the Amundsen Sea, Antarctica. *Deep-Sea Research II*, 71–76, 5–15. <https://doi.org/10.1016/j.dsr2.2012.03.006>
- Arrigo, K. R., van Dijken, G., & Long, M. (2008). Coastal southern ocean: A strong anthropogenic CO_2 sink. *Geophysical Research Letters*, 35(21), L21602. <https://doi.org/10.1029/2008GL035624>
- Arrigo, K. R., & van Dijken, G. L. (2003). Phytoplankton dynamics within 37 Antarctic coastal polynya systems. *Journal of Geophysical Research*, 108, 27–21. <https://doi.org/10.1029/2002JC001739>
- Ashley, K. E., McKay, R., Etourneau, J., Jimenez-Espejo, F. J., Condron, A., Albot, A., et al. (2021). Mid-Holocene Antarctic sea-ice increase driven by marine ice sheet retreat. *Climate of the Past*, 17(1), 1–19. <https://doi.org/10.5194/cp-17-1-2021>
- Bahr, A., Jiménez-Espejo, F., Kolasinac, N., Grunert, P., Hernández-Molina, F., Röhl, U., et al. (2014). Deciphering bottom current velocity and paleoclimate signals from contourite deposits in the Gulf of Cádiz during the last 140 kyr: An inorganic geochemical approach. *Geochemistry, Geophysics, Geosystems*, 15(8), 3145–3160. <https://doi.org/10.1002/2014GC005356>
- Bak, Y.-S., Yoo, K.-C., Lee, J. I., & Yoon, H. I. (2018). Glacial–interglacial records from sediments in Powell Basin, Antarctica. *Antarctic Science*, 30(6), 371–378. <https://doi.org/10.1017/S0954102018000408>
- Bertler, N. A. N., Mayewski, P. A., & Carter, L. (2011). Cold conditions in Antarctica during the Little Ice Age—Implications for abrupt climate change mechanisms. *Earth and Planetary Science Letters*, 308(1–2), 41–51. <https://doi.org/10.1016/j.epsl.2011.05.021>
- Björck, S., Olsson, S., Ellis-Evans, C., Håkansson, H., Humlum, O., & de Lirio, J. M. (1996). Late Holocene palaeoclimatic records from lake sediments on James Ross Island, Antarctica. *Palaeogeography, Palaeoclimatology, Palaeoecology*, 121(3–4), 195–220. [https://doi.org/10.1016/0031-0182\(95\)00086-0](https://doi.org/10.1016/0031-0182(95)00086-0)

- Christl, M., Vockenhuber, C., Kubik, P. W., Wacker, L., Lachner, J., Alfimov, V., & Synal, H.-A. (2013). The ETH Zurich AMS facilities: Performance parameters and reference materials. *Nuclear Instruments and Methods in Physics Research*, *294*, 29–38. <https://doi.org/10.1016/j.nimb.2012.03.004>
- Clem, K. R., Renwick, J. A., & McGregor, J. (2017). Large-scale forcing of the Amundsen Sea Low and its influence on sea ice and West Antarctic temperature. *Journal of Climate*, *30*(20), 8405–8424. <https://doi.org/10.1175/JCLI-D-16-0891.1>
- Cuffey, K. M., Clow, G. D., Steig, E. J., Buizert, C., Fudge, T. J., Koutnik, M., et al. (2016). Deglacial temperature history of West Antarctica. *Proceedings of the National Academy of Sciences*, *113*(50), 14249–14254. <https://doi.org/10.1073/pnas.1609132113>
- Dieckmann, G. S., Spindler, M., Lange, M. A., Ackley, S. F., & Eiken, H. (1991). Antarctic sea ice: A habitat for the foraminifer *Neogloboquadrina pachyderma*. *Journal of Foraminiferal Research*, *21*(2), 182–189. <https://doi.org/10.2113/gsjfr.21.2.182>
- Domack, E., Duran, D., Leventer, A., Ishman, S., Doane, S., McCallum, S., et al. (2005). Stability of the Larsen B ice shelf on the Antarctic Peninsula during the Holocene epoch. *Nature*, *436*(7051), 681–685. <https://doi.org/10.1038/nature03908>
- Domack, E., Levanter, A., Gilbert, R., Brachfeld, S., Ishman, S., Camerlenghi, A., et al. (2001). Cruise reveals history of Holocene Larsen ice shelf. *EOS*, *82*(213), 16–17.
- Donner, B., & Wefer, G. (1994). Flux and stable isotope composition of *Neogloboquadrina pachyderma* and other planktonic foraminifera in the Southern Ocean (Atlantic sector). *Deep-Sea Research I*, *41*(11–12), 1733–1743. [https://doi.org/10.1016/0967-0637\(94\)90070-1](https://doi.org/10.1016/0967-0637(94)90070-1)
- Dutrieux, P., De Rydt, J., Jenkins, A., Holland, P. R., Ha, H. K., Lee, S. H., et al. (2014). Strong sensitivity of Pine Island ice-shelf melting to climatic variability. *Science*, *343*(6167), 174–178. <https://doi.org/10.1126/science.1244341>
- Esper, O., & Gersonde, R. (2014). New tools for the reconstruction of Pleistocene Antarctic sea ice. *Palaeogeography, Palaeoclimatology, Palaeoecology*, *399*, 260–283. <https://doi.org/10.1016/j.palaeo.2014.01.019>
- Esper, O., Gersonde, R., & Kadagies, N. (2010). Diatom distribution in southeastern Pacific surface sediments and their relationship to modern environmental variables. *Palaeogeography, Palaeoclimatology, Palaeoecology*, *287*(1–4), 1–27. <https://doi.org/10.1016/j.palaeo.2009.12.006>
- Fryxell, G. A. (1991). Comparison of winter and summer growth stages of the diatom *Eucampia Antarctica* from the Kerguelen Plateau and south of the Antarctic convergence zone. In J. Barron, B. Larsen, et al. (Eds.), *Proc. ODP, Sci. Results* (Vol. 119, pp. 675–685). Ocean Drilling Program. <https://doi.org/10.2973/odp.proc.sr.119.139.1991>
- Gersonde, R., & Zielinski, U. (2000). The reconstruction of Late Quaternary Antarctic sea-ice distribution the use of diatoms as a proxy for sea-ice. *Palaeogeography, Palaeoclimatology, Palaeoecology*, *162*(3–4), 263–286. [https://doi.org/10.1016/S0031-0182\(00\)00131-0](https://doi.org/10.1016/S0031-0182(00)00131-0)
- Graham, A. G. C., Larter, R. D., Gohl, K., Hillenbrand, C. D., Smith, J. A., & Kuhn, G. (2009). Bed form signature of a West Antarctic ice stream reveals a multitemporal record of flow and substrate control. *Quaternary Science Reviews*, *28*(25–26), 2774–2793. <https://doi.org/10.1016/j.quascirev.2009.07.003>
- Grobe, H. (1987). A simple method for the determination of ice-rafted debris in sediment cores. *Polarforschung*, *57*(3), 123–126. Retrieved from <https://epic.awi.de/id/eprint/1071/>
- Grove, J. M. (2004). *Little ice ages: Ancient and modern* (Vol. 1). Taylor & Francis.
- Ha, H. K., Wählin, A., Kim, T., Lee, S., Lee, J., Lee, H., et al. (2014). Circulation and modification of warm deep water on the central Amundsen Shelf. *Journal of Physical Oceanography*, *44*(5), 1493–1501. <https://doi.org/10.1175/jpo-d-13-0240.1>
- Haghjipour, N., Ausin, B., Usman, M. O., Ishikawa, N., Wacker, L., Welte, C., et al. (2019). Compound-specific radiocarbon analysis by elemental analyzer–accelerator mass spectrometry: Precision and limitations. *Analytical Chemistry*, *91*(3), 2042–2049. <https://doi.org/10.1021/acs.analchem.8b04491>
- Heaton, T., Köhler, P., Butzin, M., Bard, E., Reimer, R., Austin, W., et al. (2020). Marine20—The marine radiocarbon age calibration curve (0–55,000 cal BP). *Radiocarbon*, *62*(4), 779–820. <https://doi.org/10.1017/RDC.2020.68>
- Heiden, H., & Kolbe, R. W. (1928). Die marinen Diatomeen der deutschen Südpolar-Expedition 1901–1903. In E. Drygalski (Ed.), *Deutsche Südpolar-Expedition 1901–1903, Bd. 8* (pp. 450–715). Botanik.
- Hillenbrand, C. D., Kuhn, G., Smith, J. A., Gohl, K., Graham, A. G. C., Larter, R. D., et al. (2013). Grounding-line retreat of the West Antarctic Ice Sheet from inner Pine Island Bay. *Geology*, *41*(1), 35–38. <https://doi.org/10.1130/G33469.1>
- Hillenbrand, C. D., Melles, M., Kuhn, G., & Larter, R. D. (2012). Marine geological constraints for the grounding-line position of the Antarctic Ice Sheet on the southern Weddell Sea shelf at the Last Glacial Maximum. *Quaternary Science Reviews*, *32*, 25–47. <https://doi.org/10.1016/j.quascirev.2011.11.017>
- Hillenbrand, C. D., Smith, J. A., Hodell, D. A., Greaves, M., Poole, C. R., Kender, S., et al. (2017). West Antarctic Ice Sheet retreat driven by Holocene warm water incursions. *Nature*, *547*(7661), 43–48. <https://doi.org/10.1038/nature22995>
- Hillenbrand, C. D., Smith, J. A., Kuhn, G., Esper, O., Gersonde, R., Larter, R. D., et al. (2010). Age assignment of a diatomaceous ooze deposited in the Western Amundsen Sea Embayment after the Last Glacial Maximum. *Journal of Quaternary Science*, *25*(3), 280–295. <https://doi.org/10.1002/jqs.1308>
- Hustedt, F. (1930–1966). Die Kieselalgen Deutschlands, Osterreichs und der Schweiz. In L. Rabenhorst's *Kryptogamen - Flora, Bd. 7. Die Kieselalgen, V. 1: 920p. (1930); V. 2: 845p. (1959); V. 3: 816p. (1961–1966)*.
- Hustedt, F. (1958). Diatomeen aus der Antarktis und dem Südatlantik. *Dtsch. Antarkt. ExpEditor 1938/39*, *2*, 103–191.
- Jacobs, S., Giulivi, C., Dutrieux, P., Rignot, E., Nitsche, F., & Mouginot, J. (2013). Getz Ice Shelf melting response to changes in ocean forcing. *Journal of Geophysical Research: Oceans*, *118*(9), 4152–4168. <https://doi.org/10.1002/jgrc.20298>
- Jacobs, S. S., Jenkins, A., Giulivi, C. F., & Dutrieux, P. (2011). Stronger ocean circulation and increased melting under Pine Island Glacier ice shelf. *Nature Geoscience*, *4*(8), 519–523. <https://doi.org/10.1038/ngeo1188>
- Jenkins, A., Dutrieux, P., Jacobs, S. S., McPhail, S. D., Perrett, J. R., Webb, A. T., & White, D. (2010). Observations beneath Pine Island glacier in West Antarctica and implications for its retreat. *Nature Geoscience*, *3*(7), 468–472. <https://doi.org/10.1038/ngeo890>
- Johansen, J. R., & Fryxell, G. A. (1985). The genus *Thalassiosira* (Bacillariophyceae): Studies on species occurring south of the Antarctic convergence zone. *Phycologia*, *24*(2), 155–179. <https://doi.org/10.2216/i0031-8884-24-2-155.1>
- Johnson, J. S., Bentley, M. J., & Gohl, K. (2008). First exposure ages from the Amundsen Sea Embayment, West Antarctica: The late quaternary context for recent thinning of Pine Island, Smith, and Pope glaciers. *Geology*, *36*(3), 223–226. <https://doi.org/10.1130/g24207a.1>
- Johnson, J. S., Bentley, M. J., Smith, J. A., Finkel, R. C., Rood, D. H., Gohl, K., et al. (2014). Rapid thinning of Pine Island Glacier in the early Holocene. *Science*, *343*(6174), 999–1001. <https://doi.org/10.1126/science.1247385>
- Johnson, J. S., Pollard, D., Whitehouse, P. L., Roberts, S. J., Rood, D. H., & Schaefer, J. M. (2021). Comparing glacial-geological evidence and model simulations of ice sheet change since the last glacial period in the Amundsen Sea sector of Antarctica. *Journal of Geophysical Research: Earth Surface*, *126*(6), e2020JF005827. <https://doi.org/10.1029/2020JF005827>
- Jones, T. R., Cuffey, K. M., Roberts, W. H., Markle, B. R., Steig, E. J., Stevens, C. M., et al. (2023). Seasonal temperatures in West Antarctica during the Holocene. *Nature*, *613*(7943), 292–297. <https://doi.org/10.1038/s41586-022-05411-8>
- Kim, H. J. (2012). Multibeam and sediment core: Multibeam survey. In *ANA02C cruise report* (pp. 116–117). KOPRI.

- Kim, M., Hwang, J., Kim, H. J., Kim, D., Yang, E. J., Ducklow, H. W., et al. (2015). Sinking particle flux in the sea ice zone of the Amundsen Shelf, Antarctica. *Deep-Sea Research I*, *101*, 110–117. <https://doi.org/10.1016/j.dsr.2015.04.002>
- Kim, M., Hwang, J., Lee, S. H., Kim, H. J., Kim, D., Yang, E. J., & Lee, S. (2016). Sedimentation of particulate organic carbon on the Amundsen Shelf, Antarctica. *Deep-Sea Research II*, *123*, 135–144. <https://doi.org/10.1016/j.dsr2.2015.07.018>
- Kim, M., Lee, J. I., Bak, Y. S., Hillenbrand, C. D., Yang, E. J., Montlucon, D. M., et al. (2023). *NOAA/WDS paleoclimatology-Amundsen Sea geochemistry, radiocarbon, and grain size data during the last 21 ka*. NOAA National Centers for Environmental Information. <https://doi.org/10.25921/4dss-7784>
- Kim, M., Yang, E. J., Kim, D., Jeong, J.-H., Kim, H. J., Park, J., et al. (2019). Sinking particle flux and composition at three sites of different annual sea ice cover in the Amundsen Sea, Antarctica. *Journal of Marine Systems*, *192*, 42–50. <https://doi.org/10.1016/j.jmarsys.2019.01.002>
- Kim, S., Lee, M. K., Shin, J. Y., Yoo, K. C., Lee, J. I., Kang, M. I., et al. (2022). Variation in magnetic susceptibility in the Bellingshausen Sea continental rise since the last glacial period and implications for terrigenous material input mechanisms. *Palaeogeography, Palaeoclimatology, Palaeoecology*, *594*, 110948. <https://doi.org/10.1016/j.palaeo.2022.110948>
- Kim, S. Y., Lim, D., Rebolledo, L., Park, T., Esper, O., Munoz, P., et al. (2021). A 350-year multiproxy record of climate-driven environmental shifts in the Amundsen Sea Polynya, Antarctica. *Global and Planetary Change*, *205*, 103589. <https://doi.org/10.1016/j.gloplacha.2021.103589>
- Kim, T. W., Yang, H. W., Dutrieux, P., Wählin, A. K., Jenkins, A., Kim, Y. G., et al. (2021). Interannual variation of modified circumpolar deep water in the Dotson-Getz Trough, West Antarctica. *Journal of Geophysical Research: Oceans*, *126*(12), e2021JC017491. <https://doi.org/10.1029/2021jc017491>
- Kirchner, A. E., Anderson, J. B., Jakobsson, M., O'Regan, M., Majewski, W., & Nitsche, F. O. (2012). Post-LGM deglaciation in Pine Island Bay, West Antarctica. *Quaternary Science Reviews*, *38*, 11–26. <https://doi.org/10.1016/j.quascirev.2012.01.017>
- Lamping, N., Müller, J., Esper, O., Hillenbrand, C. D., Smith, J. A., & Kuhn, G. (2020). Highly branched isoprenoids reveal onset of deglaciation followed by dynamic sea-ice conditions in the Western Amundsen Sea, Antarctica. *Quaternary Science Reviews*, *228*, 106103. <https://doi.org/10.1016/j.quascirev.2019.106103>
- Larter, R. D., Anderson, J. B., Graham, A. G., Gohl, K., Hillenbrand, C.-D., Jakobsson, M., et al. (2014). Reconstruction of changes in the Amundsen Sea and Bellingshausen Sea sector of the West Antarctic Ice Sheet since the Last Glacial Maximum. *Quaternary Science Reviews*, *100*, 55–86. <https://doi.org/10.1016/j.quascirev.2013.10.016>
- Lee, S. H., Kim, B. K., Yun, M. S., Joo, H., Yang, E. J., Kim, Y. N., et al. (2012). Spatial distribution of phytoplankton productivity in the Amundsen Sea, Antarctica. *Polar Biology*, *35*(11), 1721–1733. <https://doi.org/10.1007/s00300-012-1220-5>
- Leventer, A., Domack, E. W., Ishman, S. E., Brachfeld, S., McClennen, C. E., & Manley, P. (1996). Productivity cycles of 200–300 years in the Antarctic Peninsula region: Understanding linkages among the sun, atmosphere, oceans, sea ice, and biota. *Geological Society of America Bulletin*, *108*(12), 1626–1644. [https://doi.org/10.1130/0016-7606\(1996\)108<1626:pcoyit>2.3.co;2](https://doi.org/10.1130/0016-7606(1996)108<1626:pcoyit>2.3.co;2)
- Liu, J., Curry, J. A., & Martinson, D. G. (2004). Interpretation of recent Antarctic Sea ice variability. *Geophysical Research Letters*, *31*(2), L02205. <https://doi.org/10.1029/2003GL018732>
- Macdonald, G. J., Ackley, S. F., Mestas-Núñez, A. M., & Blanco-Cabanillas, A. (2023). Evolution of the dynamics, area, and ice production of the Amundsen Sea Polynya, Antarctica, 2016–2021. *The Cryosphere*, *17*(2), 457–476. <https://doi.org/10.5194/tc-17-457-2023>
- Manguin, E. (1957). Premier Inventaire des Diatomées de la Terre Adélie Antarctique. Espèces nouvelles. *Revue Algologique*, *3*, 111–134.
- Manguin, E. (1960). Les Diatomées de La Terre Adélie Campagne du “Commandant Charcot” 1949-1950. *Annales des Sciences Naturelles; Botanique*, *12*, 225–363.
- Martin, S. (2001). Polynyas. In J. H. Steele, K. K. Turekian, & S. A. Thorpe (Eds.), *Encyclopedia of ocean sciences* (pp. 2241–2247). Academic Press.
- Masson, V., Vimeux, F., Jouzel, J., Morgan, V., Delmotte, M., Ciais, P., et al. (2000). Holocene climate variability in Antarctica based on 11 ice-core isotopic records. *Quaternary Research*, *54*(3), 348–358. <https://doi.org/10.1006/qres.2000.2172>
- McIntyre, C. P., Wacker, L., Haghpor, N., Blattmann, T. M., Fahrni, S., Usman, M., et al. (2017). Online ¹³C and ¹⁴C gas measurements by EA-IRMS-AMS at ETH Zürich. *Radiocarbon*, *59*(3), 893–903. <https://doi.org/10.1017/RDC.2016.68>
- McKay, R. M., Dunbar, G. B., Naish, T. R., Barrett, P. J., Carter, L., & Harper, M. (2008). Retreat history of the Ross Ice Sheet (Shelf) since the Last Glacial Maximum from deep-basin sediment cores around Ross Island. *Palaeogeography, Palaeoclimatology, Palaeoecology*, *260*(1–2), 245–261. <https://doi.org/10.1016/j.palaeo.2007.08.015>
- Medlin, L., & Priddle, J. (1990). *Polar marine diatoms* (p. 214). British Antarctic Survey.
- Mezgec, K., Stenni, B., Crosta, X. V., Masson-Delmotte, C., Baroni, M., Braida, V., et al. (2017). Holocene sea ice variability driven by wind and polynya efficiency in the Ross Sea. *Nature Communications*, *8*(1), 1334. <https://doi.org/10.1038/s41467-017-01455-x>
- Miles, T., Lee, S. H., Wählin, A., Ha, H. K., Kim, T. W., Assmann, K. M., & Schofield, O. (2016). Glider observations of the Dotson Ice Shelf outflow. *Deep-Sea Research Part II*, *123*, 16–29. <https://doi.org/10.1016/j.dsr2.2015.08.008>
- Mu, L., Stammerjohn, S., Lowry, K., & Yager, P. (2014). Spatial variability of surface pCO₂ and air-sea CO₂ flux in the Amundsen Sea Polynya, Antarctica. *Elementa*, *3*. <https://doi.org/10.12952/journal.elementa.000036>
- Nakayama, Y., Menemenlis, D., Zhang, H., Schodlok, M., & Rignot, E. (2018). Origin of Circumpolar Deep Water intruding onto the Amundsen and Bellingshausen Sea continental shelves. *Nature Communications*, *9*(1), 3403. <https://doi.org/10.1038/s41467-018-05813-1>
- Ólafur, I., Hjort, C., & Humlum, O. (2003). Glacial and climate history of the Antarctic Peninsula since the Last Glacial Maximum. *Arctic Antarctic and Alpine Research*, *35*(2), 175–186. [https://doi.org/10.1657/1523-0430\(2003\)035](https://doi.org/10.1657/1523-0430(2003)035)
- Paolo, F. S., Fricker, H. A., & Padman, L. (2015). Volume loss from Antarctic ice shelves is accelerating. *Science*, *348*(6232), 327–331. <https://doi.org/10.1126/science.aaa0940>
- Parkinson, C. L. (2019). A 40-y record reveals gradual Antarctic sea ice increases followed by decreases at rates far exceeding the rates seen in the Arctic. *Proceedings of the National Academy of Sciences*, *116*(29), 14414–14423. <https://doi.org/10.1073/pnas.1906556116>
- Peragallo, M. (1921). *Deuxième Expédition Antarctique Française 1908–1910 Commandé e par le Dr. Jean Charcot. Botanique, Diatomées d'eau douce et diatomés d'eau salé e* (pp. 1–98). Masson.
- Reimer, P. J., Bard, E., Bayliss, A., Beck, J. W., Blackwell, P. G., Bronk Ramsey, C., et al. (2013). IntCal13 and Marine13 radiocarbon age calibration curves 0–50,000 years cal BP. *Radiocarbon*, *55*(4), 1869–1887. https://doi.org/10.2458/azu_js_rc.55.16947
- Rhodes, R. H., Bertler, N. A. N., Baker, J. A., Steen-Larsen, H. C., Sneed, S. B., Morgenstern, U., & Johnsen, S. J. (2012). Little Ice Age climate and oceanic conditions of the Ross Sea, Antarctica from a coastal ice core record. *Climate of the Past*, *8*(4), 1223–1238. <https://doi.org/10.5194/cp-8-1223-2012>
- Riddle, M. J., Craven, M., Goldsworthy, P. M., & Carsey, F. (2007). A diverse benthic assemblage 100 km from open water under the Amery Ice Shelf, Antarctica. *Paleoceanography and Paleoclimatology*, *22*(1). <https://doi.org/10.1029/2006PA001327>
- Rignot, E., Jacobs, S., Mouginit, J., & Scheuchl, B. (2013). Ice-shelf melting around Antarctica. *Science*, *341*(6143), 266–270. <https://doi.org/10.1126/science.1235798>

- Rignot, E., Mouginot, J., Scheuchl, B., Van Den Broeke, M., Van Wessem, M. J., & Morlighem, M. (2019). Four decades of Antarctic Ice Sheet mass balance from 1979–2017. *Proceedings of the National Academy of Sciences*, 116(4), 1095–1103. <https://doi.org/10.1073/pnas.1812883116>
- Scherer, R. P. (1994). A new method for the determination of absolute abundance of diatoms and other silt-sized sedimentary particles. *Journal of Paleolimnology*, 12(2), 171–179. <https://doi.org/10.1007/BF00678093>
- Simonsen, R. (1992). The diatom types of Heinrich Heiden in Heiden & Kolbe 1928. *Bibliotheca Diatomologica*, 24, 1–99.
- Smith, J. A., Graham, A. G. C., Post, A. L., Hillenbrand, C.-D., Bart, P. J., & Powell, R. D. (2019). The marine geological imprint of Antarctic ice shelves. *Nature Communications*, 10(1), 563. <https://doi.org/10.1038/s41467-019-13496-5>
- Smith, J. A., Hillenbrand, C.-D., Kuhn, G., Klages, J. P., Graham, A. G., Larter, R. D., et al. (2014). New constraints on the timing of West Antarctic Ice Sheet retreat in the Eastern Amundsen Sea since the Last Glacial Maximum. *Global and Planetary Change*, 122, 224–237. <https://doi.org/10.1016/j.gloplacha.2014.07.015>
- Smith, J. A., Hillenbrand, C.-D., Kuhn, G., Larter, R. D., Graham, A. G., Ehrmann, W., et al. (2011). Deglacial history of the West Antarctic Ice Sheet in the Western Amundsen Sea Embayment. *Quaternary Science Reviews*, 30(5–6), 488–505. <https://doi.org/10.1016/j.quascirev.2010.11.020>
- Smith Jr., W. O., & Barber, D. (2007). *Polynyas: Windows to the world*, (Vol. 74). Elsevier Oceanography Series.
- Sproson, A. D., Yokoyama, Y., Miyairi, Y., Aze, T., & Totten, R. L. (2022). Holocene melting of the West Antarctic Ice Sheet driven by tropical Pacific warming. *Nature Communications*, 13(1), 2434. <https://doi.org/10.1038/s41467-022-30076-2>
- Stammerjohn, S., Massom, R., Rind, D., & Martinson, D. (2012). Regions of rapid sea ice change: An interhemispheric seasonal comparison. *Geophysical Research Letters*, 39(6), L06501. <https://doi.org/10.1029/2012GL050874>
- Stammerjohn, S. E., Maksym, T., Massom, R. A., Lowry, K. E., Arrigo, K. R., Yuan, X., et al. (2015). Seasonal sea ice changes in the Amundsen Sea, Antarctica, over the period of 1979–2014. *Elementa: Science of the Anthropocene*, 3, 000055. <https://doi.org/10.12952/journal.elementa.000055>
- Stuiver, M., & Reimer, P. (1993). Extended ¹⁴C data base and revised CALIB 3.0 ¹⁴C age calibration program. *Radiocarbon*, 35(1), 215–230. <https://doi.org/10.1017/S0033822200013904>
- Thomas, D. N., Lara, R. J., Haas, C., Schnack-Schiel, S. B., Dieckmann, G. S., Kattner, G., et al. (1998). Biological soup within decaying summer sea ice in the Amundsen Sea, Antarctica. In M. P. Lizotte, & K. Arrigo (Eds.), *Antarctic sea ice biological processes, interactions, and variability*, Antarctic research series (Vol. 73, pp. 161–171). American Geophysical Union.
- Turner, J., Orr, A., Gudmundsson, G. H., Jenkins, A., Bingham, R. G., Hillenbrand, C.-D., & Bracegirdle, T. J. (2017). Atmosphere-ocean-ice interactions in the Amundsen Sea Embayment, West Antarctica. *Review of Geophysics*, 55(1), 235–276. <https://doi.org/10.1002/2016RG000532>
- Volkman, J. K. (1986). A review of sterol markers for marine and terrigenous organic matter. *Organic Geochemistry*, 9(2), 83–99. [https://doi.org/10.1016/0146-6380\(86\)90089-6](https://doi.org/10.1016/0146-6380(86)90089-6)
- Wu, L., Wang, R., Krijgsman, W., Chen, Z., Xiao, W., Ge, S., & Wu, J. (2019). Deciphering color reflectance data of a 520-kyr sediment core from the Southern Ocean: Method application and paleoenvironmental implications. *Geochemistry, Geophysics, Geosystems*, 20(6), 2808–2826. <https://doi.org/10.1029/2019GC008212>
- Yager, P. L., Sherrell, R. M., Stammerjohn, S. E., Alderkamp, A.-C., Schofield, O., Abrahamsen, E. P., et al. (2012). The Amundsen Sea Polynya International research expedition, 25 (Special issue on Antarctic oceanography in a changing world) (pp. 40–53). Retrieved from <https://www.jstor.org/stable/10.2307/24861392.2012>
- Yang, E. J., Jiang, Y., & Lee, S. (2016). Microzooplankton herbivory and community structure in the Amundsen Sea, Antarctica. *Deep-Sea Research II*, 123, 58–68. <https://doi.org/10.1016/j.dsr2.2015.06.001>
- Yang, H. W., Kim, T. W., Dutrieux, P., Wählin, A. K., Jenkins, A., Ha, H. K., et al. (2022). Seasonal variability of ocean circulation near the Dotson Ice Shelf, Antarctica. *Nature Communications*, 13(1), 1–11. <https://doi.org/10.1038/s41467-022-28751-5>
- Yoon, H. I., Park, B. K., Kim, Y., & Kim, D. (2000). Glaciomarine sedimentation and its palaeoceanographic implications along the fjord margins in the South Shetland Islands, Antarctica, during the last 6000 years. *Palaeogeography, Palaeoclimatology, Palaeoecology*, 157(3–4), 189–211. [https://doi.org/10.1016/s0031-0182\(99\)00165-0](https://doi.org/10.1016/s0031-0182(99)00165-0)
- Ziegler, M., Jilbert, T., de Lange, G. J., Lourens, L. J., & Reichert, G.-J. (2008). Bromine counts from XRF scanning as an estimate of the marine organic carbon content of sediment cores. *Geochemistry, Geophysics, Geosystems*, 9(5), Q05009. <https://doi.org/10.1029/2007GC001932>